Development of optical digital interferometry for visualizing and modelling the mass diffusion of ammonia in water in an absorption process

Ronny Rives,[a*] Daniel Salavera,[a] Juan Campos,[b] Alberto Coronas[a]

[a]Universitat Rovira i Virgili, Mechanical Engineering Department, Crever Group, Av. Països Catalans 26, 43007, Tarragona, Spain

[b]Universitat Autònoma de Barcelona; Physics Department, Optics Group, Edifici C, 08193 Bellaterra, Cerdanyola del Vallès, Spain

[*]ronny.rives@alumni.urv.cat

Keywords

Ammonia/Water mixture; Mass Diffusion, Modelling, Optical Digital Interferometry, Visualization

Abstract

This study reports the development and implementation of Optical Digital Interferometry for visualizing and modelling mass diffusion in the absorption process of ammonia in water. Absorption experiments were performed at infinite dilution of ammonia and at 293 K, 303 K, and 313 K. The method developed makes it possible to visualize the development of the mass diffusion layer and determine the evolution of concentration profiles in the ammonia/water mixture, providing new spatio-temporal data on the absorption process. A non-equilibrium model based on Fick's Second Law was used to describe the mass diffusion process. It was found that the model can successfully reproduce the experimental profiles of the ammonia concentration. The method developed also allows the simultaneous determination of mass diffusivity and mass transfer coefficients from a single experimental test. The values obtained for the mass diffusivity of ammonia in water vary from 1.54×10^{-9} m^2 s^{-1} at 293.1 K to 2.50×10^{-9} m^2 s^{-1} at 313.1 K. The relative deviations between the experimental mass diffusivity and literature values did not exceed 6.0%. The mass transfer coefficient ranges from 2.12×10^{-5} m s^{-1} at 293.1 K to 4.19×10^{-5} m s^{-1} at 313.1 K. The results show the potential of Optical Digital Interferometry for the development and validation of heat and mass transfer models used to design components in absorption refrigeration systems.

1   Nomenclature

2   Δn change in refractive index (dimensionless)

3   x, y Cartesian co-ordinates in a 2D plane (dimensionless)

4   t time (s)

5   λ laser wavelength (m)

6     $\Delta\varphi$ optical phase difference (rad)

7   L optical path of the absorption cell (m)

8   i light intensity distribution (arb. units)

9   i_0 background intensity distribution (arb. units)

10   m local contrast function (arb. units)

11   u, v spatial frequencies in the x- and y-directions (cycles per m)

12   c ammonia mass concentration in the ammonia/water mixture (kg m^{-3})

13   z vertical position from the bottom of the absorption cell (m)

14   D_{12} mass diffusivity of ammonia in water (m^2 s^{-1})

15   z_0 height of the ammonia/water mixture in the absorption cell (m)

16   k mass transfer coefficient (m s^{-1})

17   c_{eq} equilibrium concentration (kg m^{-3})

18   P_{eq} equilibrium pressure (kPa)

19   Δn_0 factor of proportionality (dimensionless)

20   T   temperature (K)

21   P   pressure (kPa)

22   *Subscripts*

23   exp   experimental

24   cal   calculated

25

26

1. Introduction

In absorption refrigeration systems, it is commonly acknowledged that the absorber is the most critical component in terms of the overall system performance, size, and first cost [1]. Consequently, the absorption process, which involves simultaneous heat and mass transfer occurring in the absorber during which the refrigerant changes phase, has been the subject of a significant amount of research [2–6].

In an original study, Kojima and Kashiwagi [2] used a holographic real-time interferometry technique to study the absorption process of ammonia in various absorbent substances. During the absorption process, the time evolution of ammonia concentration profiles in the stagnant absorbent was determined. The field of view covered by the technique was a small area near the vapour-liquid interface, around 20 mm inside the liquid bulk. The time evolution of ammonia concentration profiles in the absorbents studied was obtained by simply counting the number of interference fringe shifts in the field of view at each instance. The authors also determined the mass diffusivity of ammonia in the absorbents by fitting the experimental distribution of ammonia concentration to a theoretical model based on the one-dimensional (1D) Fick's Second Law. The main hypotheses of the mass diffusion model used were: (1) the vapour-liquid interface is saturated with ammonia throughout the absorption process, and (2) the contact time between the ammonia vapour and the absorbent is short enough for the diffusion front not to reach the bottom of the field of view.

Subsequently, Mahmoud et al. [5] and Mustafa [6] analyzed the absorption process of ammonia vapour in a stagnant pool of ammonia/water mixture using three different experimental approaches: the pressure drop method (PDM), the interface heat flux method, and optical interferometry. They compared the absorption rate values obtained from the three experimental methods used and found that the results of PDM and interferometry show reasonable agreement with each other but not with the results of the interface heat flux method.

The authors [5,6] used a Mach-Zehnder interferometer to visualize the heat and mass transfer near the vapour-liquid interface. The field of view covered was around 12 mm inside the liquid mixture. The interferograms obtained allowed

the authors to identify two diffusion layers at short absorption times. In the first layer, near the interface, mass and heat are simultaneously diffused, while in the other layer, further away from the interface, only heat is diffused. The ammonia concentration profiles were obtained by simply counting the number of interference fringe shifts in the field of view.

In their respective studies, Mahmoud et al. [5] and Mustafa [6] did not determine the mass diffusivity but did select the literature value that best describes the observed concentration profile. The authors also used a model based on the 1D Fick's Second Law valid at short absorption times. However, unlike the model used by Kojima and Kashiwagi [2], the mass diffusion model used by Mahmoud et al. [5] and Mustafa [6] did consider that the concentration at the vapour-liquid interface varied over time. The ammonia concentration at the interface was determined assuming an instantaneous equilibrium between the vapour and liquid phases at the temperature and pressure at each instant of time during the absorption process. The authors [5,6] found that fringe analysis and the mass diffusion model gave different concentration distributions. This difference was attributed to the effects of heat on fringe formation.

Previous experimental studies [2,5,6] on the absorption process show that optical techniques for the direct visualization of diffusion phenomena near the vapour-liquid interface are powerful tools for investigating the absorption process. In recent years, advancements in lasers and charge-coupled devices (CCD) have enabled optical interferometry to drastically increase the accuracy of the measurement from the typical, not very accurate, interferograms such as those used by Kojima and Kashiwagi [2] to high-resolution digital images [7,8]. At the same time, optical components, such as laser sources, beam splitters, and reflective mirrors, are now more affordable than in former times.

Nowadays, sophisticated image processing methods have become available that can be easily implemented in computational packages such as MATLAB® [9]. One of these methods, Optical Digital Interferometry (ODI), has been successfully used to determine diffusion coefficients and to visualize heat and mass transfer in liquid mixtures [10–13]. The unique feature of the ODI method is the ability to track the time evolution of temperature and concentration fields throughout the cell cross-section [14].

1 Therefore, the application of the ODI method can help reveal more valuable and
2 higher quality information about the absorption process of ammonia in
3 absorbent substances. For example, it can show the time evolution of the
4 ammonia concentration profiles in the absorbents during the absorption
5 process. These profiles can be used to assess whether a specific boundary
6 condition or model is suitable for describing ammonia mass diffusion during the
7 absorption process correctly. Moreover, the time evolution of ammonia
8 concentration profiles is also useful for the development and validation of more
9 complex heat and mass transfer models that can be used for screening suitable
10 absorbents for this natural refrigerant.

11 The ODI method can also be used to determine the mass diffusivity of natural
12 refrigerants in absorbent substances, an essential transport property, before
13 going on to make a detailed study of the heat and mass transfer performance of
14 new working pairs so that different types of absorbers can be properly
15 designed.

16 Recently, our research group [15] implemented a new experimental setup to
17 investigate the behaviour of the absorption process and determine the mass
18 diffusivity of ammonia in absorbent substances using the ODI method. Despite
19 the significant benefits derived from the application of the ODI method, this
20 method is currently not widely used to investigate the absorption process. In our
21 opinion, the main obstacle lies not in the fundamental limitations of the
22 technique but in the lack of adequately developed experimental procedures,
23 incomprehension of the mathematical formalism, and the lack of familiarity with
24 the data processing steps.

25 Therefore, this paper reports the development and implementation of Optical
26 Digital Interferometry for investigating the absorption process of natural
27 refrigerants in absorbent substances for absorption refrigeration systems. In
28 particular, the main objectives are to visualize and model the time evolution of
29 concentration profiles of ammonia refrigerant in the conventional absorbent,
30 water. A mass diffusion model based on the 1D Fick's Second Law was used to
31 describe the ammonia mass diffusion in the ammonia/water mixture. The mass
32 diffusion model – namely, the non-equilibrium model – is unlike previous models

in the literature [2,5,6] in that it uses different key assumptions and boundary conditions.

2. Experimental approach

2.1. Materials, setup, and experimental procedure

Anhydrous ammonia (purity 99.98%, CAS no. 7664-41-7) was obtained from Carburos Metálicos and was used directly without any further purification. Deionized water with a MilliQ reagent-grade was obtained from the laboratories of the Universitat Rovira i Virgili (URV), and it was degassed to avoid the formation of bubbles, which can seriously affect the ammonia concentration distribution in water.

The experimental setup (Figure 1) consisted of an absorption test loop based on the Pressure Drop Method and an optical system for visualization that used the Mach-Zehnder interferometer. The main components of the test loop were the absorption cell (see Figure 2), in which the absorption process took place, and the cylindrical tank, which contained the ammonia vapour that fed the absorption cell during the absorption process. Three pressure transducers (Wika, model S20) measured the pressure in the test loop, two in the absorption cell and one in the cylindrical tank. The temperature in the absorption cell was measured with five 4-wires Pt100 probes, one of which was placed in the vapour phase while the other four were placed at equidistant depths in the liquid phase. The probes in the liquid phase allowed us to obtain a temperature profile for the investigation of the thermal behaviour of the ammonia/water mixture. The temperature of the absorption cell was controlled by a circulating bath (Huber, model Pilot One), which pumped distilled water through a copper cooling coil placed around the absorption cell. Also, another 4-wires Pt-100 probe was placed in the cylindrical tank. All the temperature probes and pressure transducers were connected to the data acquisition system (Keysight/Agilent 34972A).

Before experiments, the non-condensable gases trapped in the absorption test loop were removed by a vacuum pump (Comecta-Ivymen). Then, ammonia vapour and water were charged into the cylindrical tank and the absorption cell, respectively. The ammonia vapour was taken directly from an external reservoir

1   until the desired pressure value (≈1 atm) in the cylindrical tank was reached.

2   This pressure value was selected to guarantee infinite dilution conditions for the

3   ammonia absorption process in water. Meanwhile, the mass of water (≈30 g) in

4   each experimental run was used in such a way as to allow good visibility of the

5   vapour-liquid interface and maximum use of the optical windows to visualize the

6   absorption process. The mass of water used in each experimental run was

7   weighed on a Mettler AE 260 DeltaRange digital mass balance (resolution ± 0.1

8   mg). Then, it was carefully fed into the absorption cell in vacuum conditions
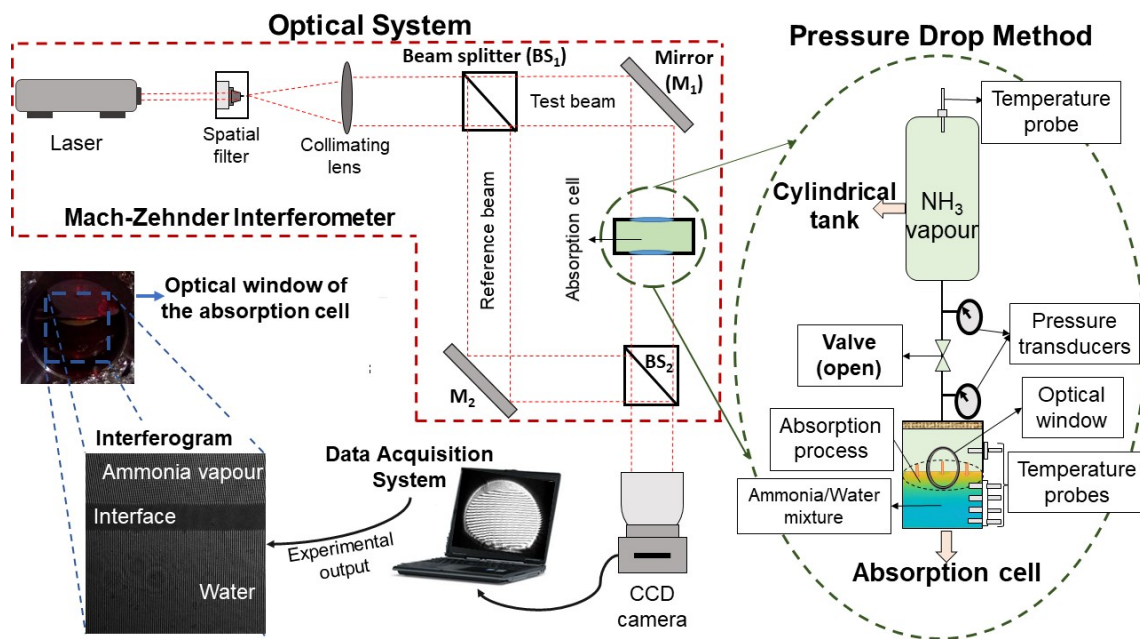
9   through the injection line.

10

11 *Figure 1. Schematic of the experimental setup*

12   Initially, the absorption cell and the cylindrical tank were connected by a closed

13   valve, which did not allow contact between the ammonia vapour (at higher

14   pressure) and the absorbent water (in vacuum conditions). To start the

15   absorption experiments, the valve between the absorption cell and the

16   cylindrical tank was opened. Consequently, the ammonia vapour expanded into

17   the absorption cell, and the absorption process began. The valve was kept open

18   throughout the experiment so the ammonia vapour feed was continuous. The

19   temperature and pressure of the absorption cell and the cylindrical tank were

20   continuously monitored. Absorption experiments were performed at

21   temperatures of 293 K, 303 K and 313 K.

Figure 1 also shows the optical system (Mach-Zehnder interferometer) used for the visualization of the process. Here, the beam from a He-Ne laser (λ = 632.8 nm, Thorlabs, HRS015B) was used as a light source. First, the laser beam was expanded, filtered and collimated. Then, the collimated beam was divided by a beam splitter (BS_1), which refracted half of the amplitude and transmitted the other half. The resulting beams travelled through different optical paths in the system. One of the beams – the reference beam – passed through the ambient air. The other beam – the object or test beam – passed through the absorption cell (see Figure 2). Finally, the two beams were recombined by a second beam splitter (BS_2) and imaged on a CCD camera (Basler, piA1000-60gm) by an objective lens (Fujinon, HF75HA-1B). The optical paths of the two beams were different so an optical phase difference was generated. As a result, an image presenting interference fringes, called an interferogram or fringe pattern, was observed.

The resulting interferogram was recorded by a CCD camera with a 1000 x 1000 pixels sensor. The resolution of the imaging system was around 9.0 µm per pixel. The image acquisition time step was varied from 30 s at the beginning of the experiment to 300s at the end. All optical elements were mounted on mechanical platforms so that they could be accurately adjusted. In addition, the Mach-Zehnder interferometer (MZI) and the absorption cell were mounted on a special optical table (Nexus Breadboard, 750 mm x 900 mm x 60 mm) with a vibration isolation system.

Figure 2 shows the schematic design of the absorption cell used for the experiments. The optical path length inside the liquid bulk was 35.4 ±0.3 mm. At the top of the absorption cell, a Teflon® mesh was added so that the ammonia vapour could be uniformly distributed over the entire vapour-liquid interface. The absorption cell was equipped with two optical sapphire windows (model SAW24, diameter 25.40 mm, thickness 2.30 mm, from Lasing S.A) for the visualization of the absorption process.
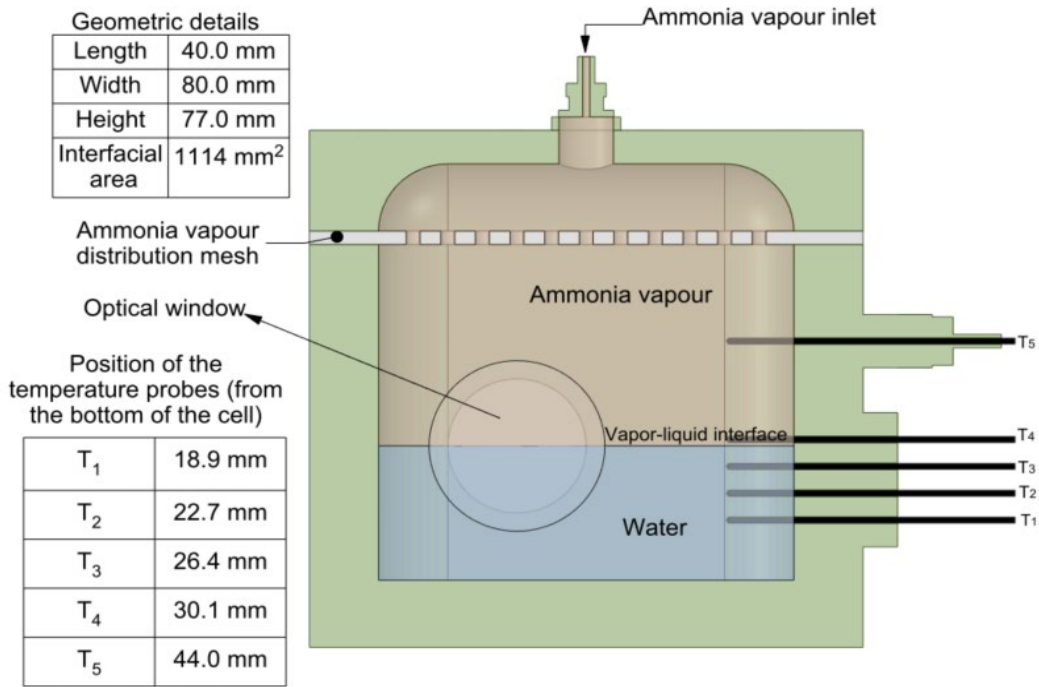
Geometric details

Length	40.0 mm
Width	80.0 mm
Height	77.0 mm
Interfacial area	1114 mm²

Ammonia vapour inlet

Ammonia vapour distribution mesh

Optical window

Ammonia vapour

T_5

Vapor-liquid interface T_4

T_3

T_2

Water T_1

Position of the temperature probes (from the bottom of the cell)

T_1	18.9 mm
T_2	22.7 mm
T_3	26.4 mm
T_4	30.1 mm
T_5	44.0 mm

Figure 2. Schematic of the absorption cell

2.2. Optical Digital Interferometry

Interferograms obtained during absorption experiments implicitly provide the optical phase difference ($\Delta\varphi(x,y,t)$) between the test beam and reference beam of the MZI. In turn, $\Delta\varphi(x,y,t)$ can be related to the change in the refractive index ($\Delta n_{exp}(x,y,t)$) of the ammonia/water mixture as:

$$\Delta n_{exp}(x,y,t) = \frac{\lambda}{2\pi L}\Delta\varphi(x,y,t) \qquad (1)$$

where *L* is the optical path inside the ammonia/water mixture.

However, the experimentally observed quantity is the light intensity in each pixel of the interferogram and not the optical phase difference itself. Therefore, a suitable processing method, such as Optical Digital Interferometry (ODI), should be used to extract the optical phase from the measure of light intensity distribution in the interferograms. For this purpose, we used the ODI method in combination with the Fourier transform technique [16]. The mathematical description of the optical phase extraction procedure is shown below.

2.2.1. Optical phase extraction from the interferograms

The measured light intensity distribution in the interferograms can be expressed as:

1 $$i(x,y) = i_0(x,y) + m(x,y) \cdot cos\,[2\pi u_0 x + \Delta\varphi(x,y)] \qquad (2)$$

2 where $i_0(x,y)$ represents the background variation and $m(x,y)$ is related to the

3 local contrast of the pattern. $2\pi u_0 x$ is the linear phase introduced by the tilted

4 mirror, u_0 is associated with the spatial frequency of the fringes and $\Delta\varphi(x,y)$ is

5 the remaining optical phase difference between the interferometer arms.

6 The fringe-pattern formula (Eq. (2)) can be written as one term around zero

7 frequency and two terms around frequency u_0:

8 $$i(x,y) = i_0(x,y) + \exp[j2\pi u_0 x].d(x,y) + \exp[-j2\pi u_0 x].d^*(x,y) \quad (3)$$

9 where:

10 $$d(x,y) = \tfrac{1}{2}m(x,y) \cdot \exp[j\Delta\varphi(x,y)] \qquad (4)$$

11 with $j = \sqrt{-1}$ and * denoting the complex conjugate. The terms of interest in Eq.

12 (3) are $d(x,y)$ and $d^*(x,y)$, which contain the optical phase difference term.

13 Then, Eq. (3) had to be Fourier transformed to give:

14 $$I(u,v) = I_0(u,v) + D(u,v) * \delta(u - u_0) + D^*(-u,-v) * \delta(u + u_0) \quad (5)$$

15 where $*$ represents the convolution operator, and the term D is the Fourier

16 transform of $d(x,y)$. D and D* were placed symmetrically around the origin at

17 frequencies $\pm u_0$ respectively. These terms contain equivalent information about

18 the optical phase difference. Therefore, the next step was to filter out either one

19 of the two spectra. By applying a Gaussian filter centred at $-u_0$, all frequencies

20 except those that belong to D* were filtered out. Then, D* was shifted to the

21 zero frequency, and the inverse Fourier transform was applied, so the term

22 $d^*(x,y)$, defined in Eq. (3), was obtained. Finally, the optical phase difference

23 between the interferometer arms (without the linear phase introduced by the

24 mirror) was calculated from $d^*(x,y)$ as:

25 $$\Delta\varphi(x,y) = arctan\left\{\frac{Im[d^*(x,y)]}{Re[d^*(x,y)]}\right\} \qquad (6)$$

26 where $Im[d^*(x,y)]$ and $Re[d^*(x,y)]$ denote the real part and the imaginary part,

27 respectively. After these steps, the results were a set of two-dimensional (2D)

28 optical phase map images wrapped into [-π, π] range. The next step in the

29 image processing was to select a reference image. This reference image was

30 subtracted from each of the following images to separate the value of interest.

In this study, we are interested in the refractive index variations caused by changes in ammonia concentration in the water. Thus, the reference interferogram was taken as the last image recorded just before the beginning of the absorption process.

2.2.2. Phase unwrapping

Optical phase maps need to be unwrapped so that a continuous natural phase can be constructed [10]. The procedure begins with the selection of a pixel where it is assumed that the wrapped phase is equal to the unwrapped phase. Selecting a suitable reference pixel is a very important step because it modifies the shape of the unwrapped phase profile and, therefore, the concentration profile. In diffusion experiments involving liquid-liquid systems, the reference pixel is generally located at the centre of the optical phase maps [10,11,13], since the concentration profiles are symmetric with respect to that position.

However, in diffusion experiments involving vapour-liquid systems, as in the present study, the concentration profiles are not symmetric to the centre of the optical phase maps. In this case, the reference pixel can be conveniently located at the vapor-liquid interface or at the bottom of the field of view, depending on the boundary conditions used to describe the mass diffusion in the absorption process. For example, Mahmoud et al. [5] and Mustafa [6] considered that the ammonia concentration at the vapour-liquid interface varies with time. Consequently, the refractive index of the ammonia/water mixture near the vapour-liquid interface must also change and it is not appropriate to select a reference pixel located at that position. Nevertheless, for short absorption times, when the diffusion front has not reached the bottom of the field of view, there is no change in the refractive index of the ammonia/water mixture at the bottom of the field of view. Therefore, like Wylock et al. [7], here we have used a reference pixel located at the bottom of the field of view.

Two-dimensional phase unwrapping could be demanding, especially for noisy fringe images, for which sophisticated unwrapping techniques are required [10]. In our case, the 2-D phase maps were generally of good quality, so we adopted an approach based on the method described by Kreis [17]. The unwrapping procedure started from the reference pixel. The optical phase of this pixel was compared with a neighbouring pixel. If the magnitude of the difference between

the two neighboring pixels was less than π, the optical phase remained unchanged. If the difference between two pixels was less than -π, then 2π was added to the wrapped phase; otherwise, if the difference was more than π, 2π was subtracted from the wrapped phase at that pixel [18]. Each pixel was compared to a previously validated one in the horizontal and vertical directions, and this iterative procedure was performed over the full wrapped phase map. In the next image-processing step, the unwrapped phase maps were converted into refractive index maps by applying Eq. (1).

2.2.3. Image processing steps

Figure 3 shows the main image processing steps of the ODI method combined with the Fourier transform technique for investigating mass diffusion in ammonia/water mixtures.

1. Two-dimensional (2D) Fourier transform is applied to each experimental interferogram (Figure 3(a)). The result is a spectrum with three peaks in the Fourier domain (Figure 3(b)).
2. One of the lateral peaks is selected using a Gaussian filter, and then, the selected peak is moved towards the origin of the Fourier domain (Figure 3(c)).
3. The inverse Fourier transform is applied to the filtered sideband, and the result is an optical phase map wrapped in the range [-π, π] (Figure 3(d)).
4. The wrapped phase map is cropped, the reference pixel is selected, and an unwrapping procedure is applied. Thus, an unwrapped optical phase map, as shown in Figure 3(e) is obtained.
5. Finally, the unwrapped optical phase map is converted into a refractive index map (Figure 3(f)) by applying Eq. (1).

An image processing code was developed in Matlab [9], which makes the above steps easy to implement, including the Fourier transform technique (FFT), and extract the refractive index change maps from the experimental interferograms.
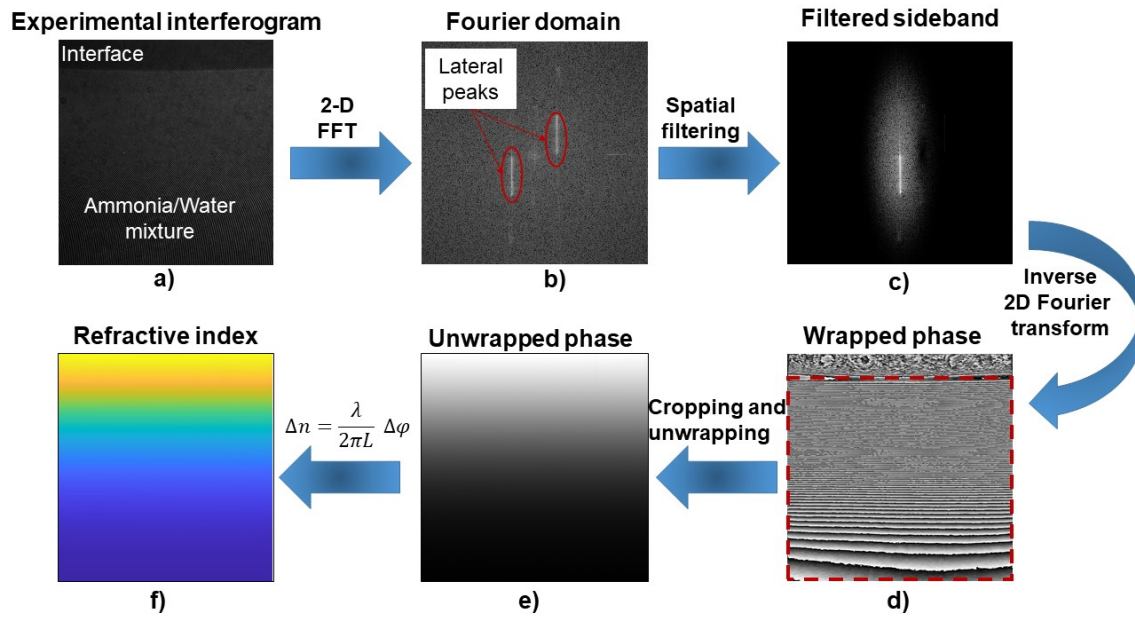
Figure 3. Image processing steps: (a) an interferogram (experimental output); (b) image after applied 2D fast Fourier transform (FFT); (c) filtered sideband using a Gaussian filter; (d) wrapped phase map; (e) unwrapped phase map; (f) refractive index field of the ammonia/water mixture in the field of view of the absorption cell.

3. Visualization of the mass diffusion layer and the experimental profiles of the refractive index change

Figure 4 shows two interferograms obtained at different instances during a typical experimental run. The horizontal black strip observed corresponds to the area of the vapour-liquid interface. The meniscus shape of the interface deflects the test beam light in this area, so this area appears in black in the interferograms [7].

Before the inlet valve of the absorption cell was opened (see Figure 1), the interference fringes were vertical, as shown in Figure 4(a). In our optical system, one of the mirrors (M_2 in Figure 1) was tilted to produce a linear optical phase difference in the horizontal direction. Thus, vertical interference fringes were observed even if the fluids in the absorption cell were optically uniform.

Then, as soon as the ammonia absorption process started, an additional optical phase difference was established between both arms of the interferometer. This additional difference was due to the local distribution of the refractive index of the ammonia/water solution. An interferogram recorded a few minutes after the

13

start of the absorption process is presented in Figure 4 (b). It shows that the fringes were bent in the region of the image corresponding to the ammonia/water solution just below the interface. This means that the variation of the refractive index was greater in that region than in a deeper region of the liquid bulk. Moreover, the interface area is also observed to thicken between Figure 4 (a) and (b). This thickening was caused by the expansion of the ammonia vapour, which was initially at a higher pressure than the water in the absorption cell, and it is mainly observed during the first minutes of the absorption process. After this time, the pressure began to decrease due to the absorption of ammonia in the water, and it was observed that the thickness of the interface remained stable until the end of the experiments.
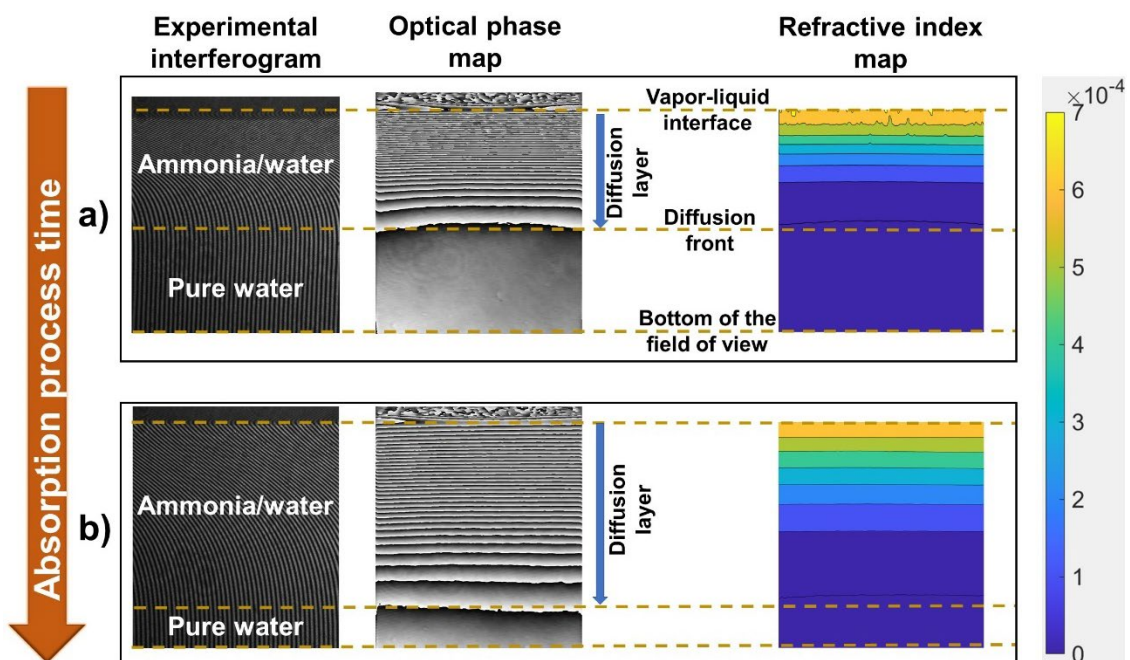

a) Before the absorption process   *b) During the absorption process*
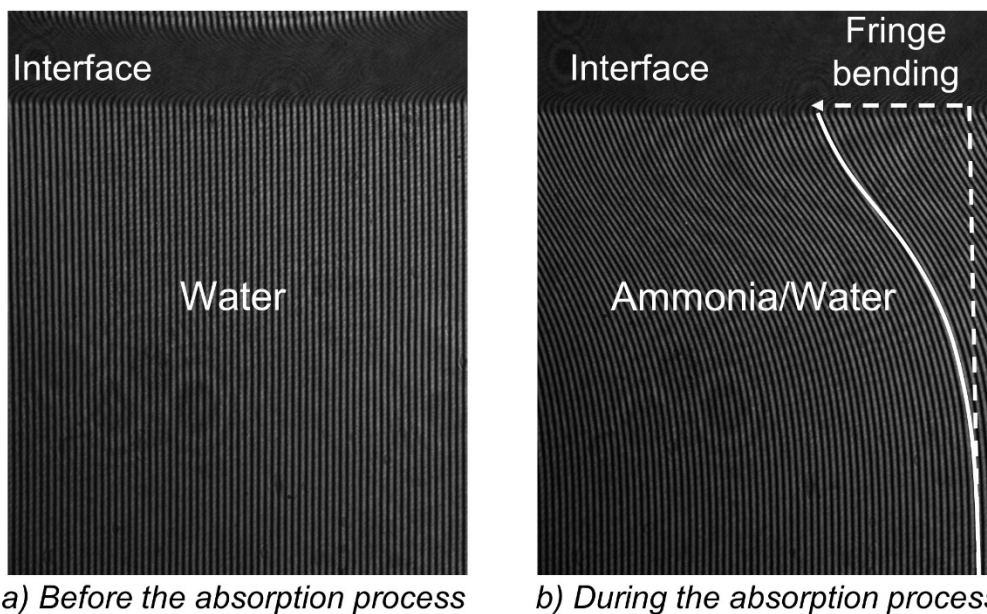
Figure 4. Experimental interferograms or fringe images

At the scale of the interferogram, the optical phase difference between the reference beam and the test beam of the MZI leads to a time and space evolution of the fringe positions. By following this evolution, the MZI can accurately detect local variations in the refractive index during mass diffusion in the absorption process [7]. In this way, the experimental setup visualizes the formation and evolution of the mass diffusion layer inside the ammonia/water mixture.

Figure 5 shows the development of the mass diffusion layer during the absorption process of ammonia in water at 313.1 K at different times. Two

1 regions of a similar size can be identified in the interferogram shown in Figure 5

2 a). In the region closest to the vapour-liquid interface, the fringes bend to the left

3 because of the mass diffusion of ammonia into the water bulk. While in the

4 region furthest from the interface and therefore closest to the bottom of the field

5 of view, the fringes remain vertical. This suggests that there is a layer within the

6 liquid bulk in which the diffusive transport of ammonia in water takes place.

7 Outside this mass diffusion layer, no ammonia is present and, therefore, the

8 liquid bulk is pure water. However, as the absorption process progresses, the

9 mass diffusion layer gets thicker (Figure 5(b)). After a sufficiently long time, the

10 diffusion front reaches the bottom of the field of view.

12 *Figure 5. Evolution of the mass diffusion layer at different times during the absorption*

13 *process of ammonia in water at 313.1 K: a) 10 minutes; b) 14 minutes.*

14 Figure 5 also shows the corresponding (wrapped) optical phase and refractive

15 index maps. Optical phase maps are very useful for identifying the *"preferred"*

16 direction of the mass diffusion layer. In this case, mass diffusion occurs in the

17 vertical direction, from the vapour-liquid interface to the bottom of the field of

18 view.

19 The ODI method makes it possible to increase measurement accuracy by

20 providing information about concentration distribution throughout the diffusion

21 path. It provides a two-dimensional concentration field, although the distribution

22 can be considered one-dimensional (1D), as confirmed by the refractive index

maps in Figure 5. To apply 1D mathematical description of measurements, the 2D map of the refractive index change is averaged in the horizontal direction. This averaging increases the reliability of the extracted profiles because it suppresses local noise, which is otherwise observable, without applying additional filters.

Figure 6 shows the evolution of the experimental profiles of the refractive index change (Δn) in the ammonia/water mixture during the absorption process at 313.1 K. At absorption times of 5 and 7 minutes, the combined effects of changes in concentration and temperature and thickening of the interface caused a high refractive index gradient that led to squeezing of the fringes of unwrapped phase, resulting in unresolvable phase steps. This caused a *"deformation"* in the part of the refractive index change profiles near the vapor-liquid interface that did not correctly reflect the *"real"* concentration profiles in the mixture. Nonetheless, after a few minutes, the interface thickness and temperature stabilized in the experiments, so the refractive index change profiles were considered to be affected only by concentration changes, as discussed in Appendix A.
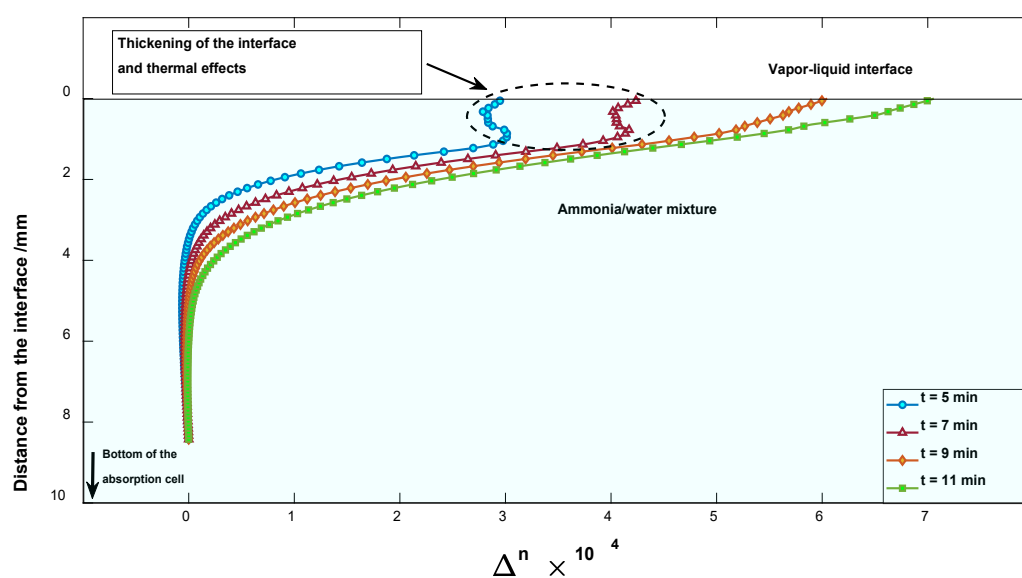
Figure 6. Evolution of the experimental profile of the refractive index change (Δn) in the ammonia/water mixture during the absorption process at 313.1 K

Figure 6 also shows that as the absorption process progresses and more ammonia passes from the vapour phase to the liquid phase, the difference in Δn between the upper and lower regions inside the ammonia/water mixture

16

increases. This difference increases until the diffusion front reaches the lower region of the field of view. Then, the difference gradually begins to decrease as the interface tends to saturate, and the diffusion front continues until it reaches the lower region of the field of view. The refractive index change profiles shown in Figure 6 are useful for evaluating specific modelling approaches to the absorption process of ammonia in water, as discussed below.

4. Modelling the mass diffusion in the absorption process

Modelling the mass diffusion in the absorption process of ammonia in water is quite a demanding task due to the presence of complex physical phenomena, which include the possible evolution of the heat of absorption, liquid convection, and the possible change in thermophysical properties of the liquid [19]. Nevertheless, the effect of these complex phenomena can be minimized with a well-designed experimental setup and suitable experimental conditions. In the literature [2,5,6,19–22], different mathematical models based on a simplified mass diffusion equation have been used to describe the time-dependent behaviour of the absorption process. These models and their solutions have different interface thermodynamic conditions, assumptions, and parameter estimation algorithms [22]. The present study makes the following assumptions:

1. Mass diffusion in the ammonia/water mixture is one-dimensional, and there is no convective flow in the absorption process of ammonia in water [2–6,20].

2. For the diffusion analysis, the temperature in the absorption cell is considered constant [21]. In the experimental setup implemented, the dimensions of the absorption cell and the capacity of the thermal control circuit facilitate rapid heat transfer between the ammonia/water mixture and the external fluid of the thermal control circuit, which keeps the temperature practically constant during the absorption process.

3. The ammonia is highly diluted in the water (the ammonia mass fraction in the ammonia/water mixture does not exceed 0.007 in the absorption experiments). Thus, the relevant thermophysical properties of the mixture do not significantly change during the absorption process [19].

4. The amount of ammonia absorbed in water is too small to cause a noticeable increase in the volume of the liquid phase. Therefore, the

17

1 　　　　liquid phase's height in the absorption cell is assumed to be constant
2 　　　　during the absorption process [21].

3 　On the basis of the above assumptions, the mass diffusion in the
4 　ammonia/water mixture can be obtained using Fick's Second Law as:

5
$$\frac{\partial c}{\partial t} = D_{12} \frac{\partial^2 c}{\partial z^2} \tag{7}$$

6 　where c [kg m^{-3}] is the ammonia mass concentration in the ammonia/water
7 　mixture; z [m] is the vertical position from the bottom of the absorption cell; t [s]
8 　is time; and D_{12} [m^2 s^{-1}] is the mass diffusivity of ammonia in water. Figure 7
9 　displays a schematic of the boundary conditions (BCs) used to model the mass
10 　diffusion in the absorption process of ammonia in water.
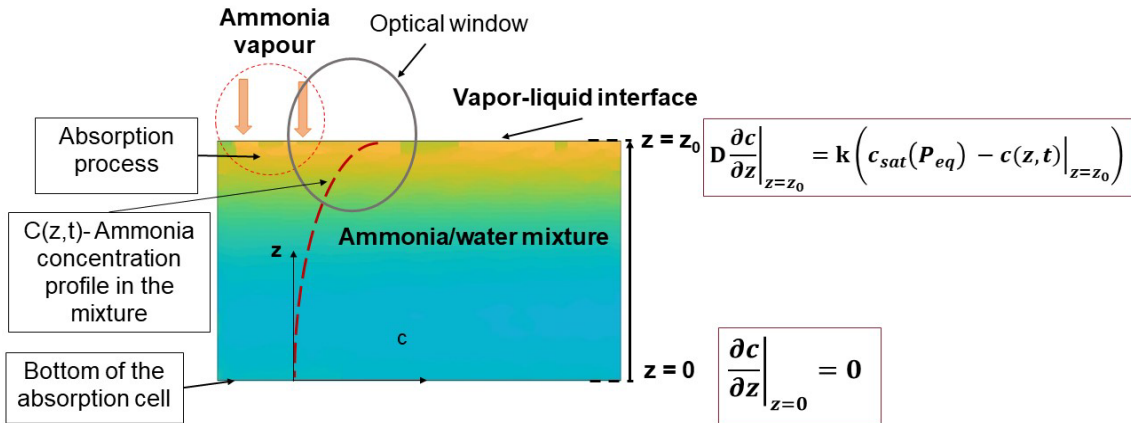
12 　*Figure 7. Schematic of the boundary conditions used to model mass diffusion in the*
13 　*absorption process of ammonia in water*

14 　To solve Eq. 7, one initial condition and two boundary conditions are required.
15 　Before the absorption process, the water contains no ammonia (i.e. the
16 　absorbent is pure water). Thus, in all the experiments, the initial condition is
17 　given by:

18
$$c(z,t)|_{t=0} = 0 \qquad (0 \leq z \leq z_0) \tag{8}$$

19 　One boundary condition can be conveniently located at the bottom of the
20 　absorption cell and the other at the vapour-liquid interface.

21 　At the bottom of the absorption cell, two different options can be considered
22 　depending on the contact time and the mass transfer rate between the vapour
23 　and liquid phases. Here, we have assumed that the diffusion front does not

reach the bottom of the absorption cell. Therefore, the diffusion can be considered as occurring in a semi-infinite medium, and the boundary condition is expressed as:

$$c = 0 \qquad (z = 0 \quad and \quad t \geq 0) \tag{9}$$

The literature reports three main boundary conditions at the vapour-liquid interface; namely, equilibrium, quasi-equilibrium, and non-equilibrium [22,23].

Here, we have adopted a non-equilibrium boundary condition that more realistically describes the mass diffusion phenomena in the absorption process of ammonia in water in our experimental setup. Therefore, the ammonia mass transfer flux at the interface is assumed to be proportional to the difference between the saturation concentration under the equilibrium pressure and the existing concentration at the interface [23]:

$$D \left. \frac{\partial c}{\partial z} \right|_{z=z_0} = k \left(c_{sat}(P_{eq}) - c(z,t)|_{z=z_0} \right) \tag{10}$$

where k [m s^{-1}] is the mass transfer coefficient, and 1/k represents the interfacial resistance.

The solution of Fick's Second Law (Eq. 7) subjected to the initial (Eq. 8) and boundary conditions (Eqs 9 and 10) is given by Crank [24]:

$$c^*(z,t) = \text{erfc}(\xi) - \exp(\text{h}(z_0 - z) + \text{h}^2 D_{12} t) \, \text{erfc}\left(\xi + \text{h}\sqrt{D_{12} t}\right) \tag{11}$$

where z_0 is the height of the ammonia/water mixture in the absorption cell, $\xi = \frac{z_0 - z}{2\sqrt{D_{12} t}}$, h = k/D$_{12}$, $c^*(z,t) = c(z,t)/c_{eq}$, and c_{eq} is the equilibrium concentration.

Thus, the concentration changes in the ammonia/water mixture between the initial or reference time, $t_{ref} = 0$, and any other time during the absorption process, t, can be expressed as:

$$\Delta c^*(z,t) = c^*(z,t) - c^*\left(z, t_{ref} = 0\right) = c^*(z,t) - 0 = c^*(z,t) \tag{12}$$

since initially, there is no ammonia in the water.

4.1. Determination of the mass diffusivity of ammonia in water

The changes in ammonia concentration may be related to changes in the refractive index of the ammonia/water mixture. On the assumption that they are

linearly related [25] (for the concentration ranges found in our experiments), the refractive index variation profile can be calculated as:

$$\Delta n_{cal}(z,t) = \Delta n_0 \cdot \Delta c^*(z,t) \tag{13}$$

where Δn_0 is a factor of proportionality which accounts for the equilibrium concentration and the mean value of the derivative of the refractive index on concentration (so-called concentration contrast factor) for the experimental concentration range. Since this factor is unknown, it is determined simultaneously with the mass diffusivity and mass transfer coefficient using a non-linear least-squares minimization of the deviation between experimental ($\Delta n_{exp}(z,t)$) and calculated ($\Delta n_{cal}(z,t)$) refractive index profiles as:

$$\Phi = \sum_{i,j}[\Delta n_{exp}(z_i,t_j) + \Delta n_{cal}(z_i,t_{\text{ref}}) - \Delta n_{cal}(z_i,t_j)]^2 \tag{14}$$

Several minimization algorithms can be found in the literature and are available in commercial software packages such as MATLAB ® [26]. In the present study, the Nelder-Mead (simplex) [10,27] and Levenberg-Marquardt [22] algorithms were used to determine the unknown parameters. The minimization procedure was based on the sequential application of both algorithms to benefit from their respective advantages. Thus, we divided the regression procedure into two steps to accelerate the convergence. The first step aimed to search for good initial guesses using the Nelder-Mead (simplex) algorithm. The second step was the iterative process to minimize Φ, which used the initial guesses obtained in the first step. The second step was performed using the Levenberg-Marquardt algorithm.

5. Results and Discussion

Figure 8 shows the ammonia concentration profiles observed and calculated during the absorption process of ammonia in water, at 313.15 K. Also shown in the figure are the regressed parameters and the coefficient of determination (R^2), which was calculated as:

$$R^2 = 1 - \frac{\sum_{i=1}^{N}[c^*_{exp}(i) - c^*_{cal}(i)]^2}{\sum_{i=1}^{N}[c^*_{exp}(i) - \overline{c^*}_{exp}]^2} \tag{15}$$

where c^*_{exp} is the experimental concentration, c^*_{calc} the calculated concentration, and $\overline{c^*}_{exp}$ is the average value of the experimental concentration.
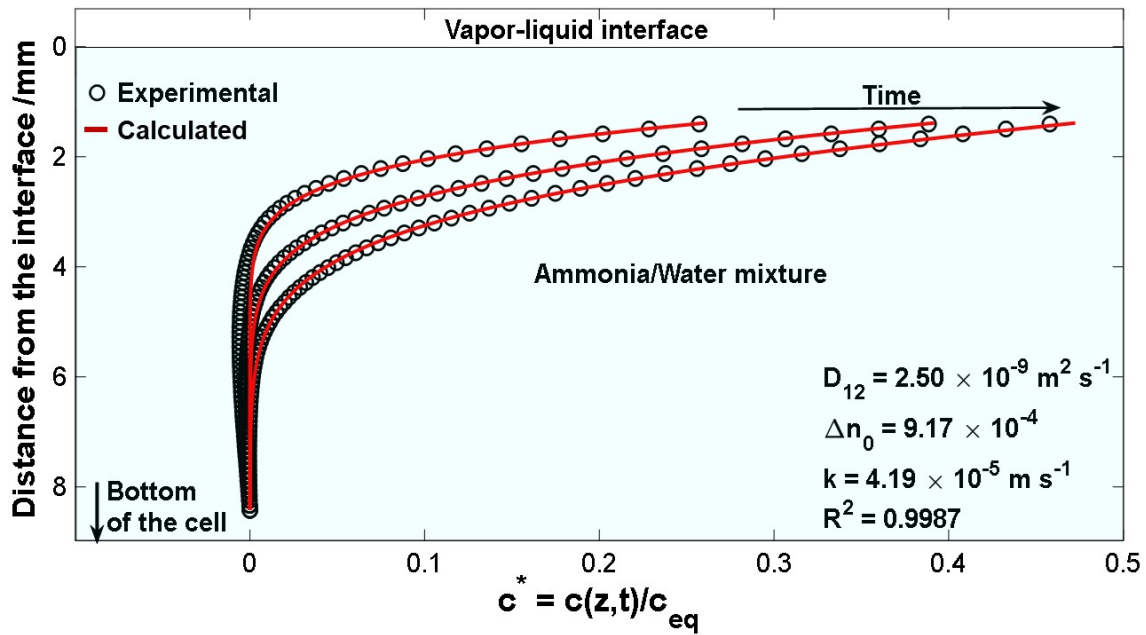
Figure 8. Experimental and calculated profiles of the ammonia concentration during the mass diffusion process in the ammonia/water mixture at 313.15 K

A coefficient of determination (R^2) close to 1, as shown in Figure 8, indicates that the mass diffusion model used satisfactorily reproduces the experimental profiles of the ammonia concentration in the ammonia/water mixture.

In Figure 8, the part of the concentration profiles near the vapour-liquid interface that could be affected by interface thickening and temperature variations at the beginning of the absorption process has been excluded. The flexibility of the ODI method makes it possible to exclude the *"deformed"* part of the experimental profiles without losing sensitivity due to the large number of experimental points it provides. Note that the number of spatial pixel points in the experimental data set is around 800, and the number of images acquired in a typical experimental run is 20, giving a total of 16000 experimental points to determine only three unknown parameters (D_{12}, k, and Δn_0).

Table 1 lists the main results of the present study. As expected, the mass diffusivity increases with temperature and ranges from 1.54 x 10^{-9} m^2 s^{-1} at 293.1 K to 2.50 x 10^{-9} m^2 s^{-1} at 313.1 K. The relative expanded uncertainty in our diffusivity measurements, $U_r(D_{12})$, do not exceed 3% with a confidence level of 0.95 (coverage factor k = 2). As shown in the table, the mass transfer coefficient also increases with temperature and it ranges from 2.12 x 10^{-5} m s^{-1} at 293 K to 4.19 x 10^{-5} m s^{-1} at 313.1 K. Unlike the mass diffusivity and mass

21

1   transfer coefficient, the factor of proportionality Δn_0 decreases with temperature,

2   which is consistent with the expected behaviour of the equilibrium concentration

3   for the mixture studied. The coefficient of determination (R^2) shown in Table 1

4   indicates that the mass diffusion model used provides satisfactory results at all

5   temperatures studied.

6   *Table 1. Mass diffusivity (D_{12}) and mass transfer coefficient (k) in the ammonia/water*
7   *mixture at different experimental conditions*

T /K	P /kPa	D_{12} x 10^9 /m^2 s^{-1}	k x 10^5 /m s^{-1}	Δn_0 x 10^3	R^2
293.1 ± 0.7	14 ± 4	1.54 ± 0.04	2.12 ±0.05	2.50 ± 0.06	0.9949
303.0 ± 0.5	29 ± 5	1.84 ± 0.04	3.04 ± 0.07	2.14 ± 0.05	0.9985
313.1 ± 0.3	70 ± 3	2.50 ± 0.07	4.19 ± 0.10	0.92 ± 0.03	0.9987

8   Figure 9 shows the deviations between the determined mass diffusivity and the

9   values from the literature at different temperatures. Although there are several

10   experimental studies available in the literature, most of the diffusivity data for

11   the ammonia/water mixture under conditions of infinite dilution are out of date.

12   We found that only Frank et al. [28] have reported recent data at the

13   temperatures studied here. They used a Taylor Dispersion Technique to

14   determine the diffusion coefficients of ammonia in water at different

15   temperatures, at atmospheric pressure, and in the concentration range between

16   0 and 0.312.

17
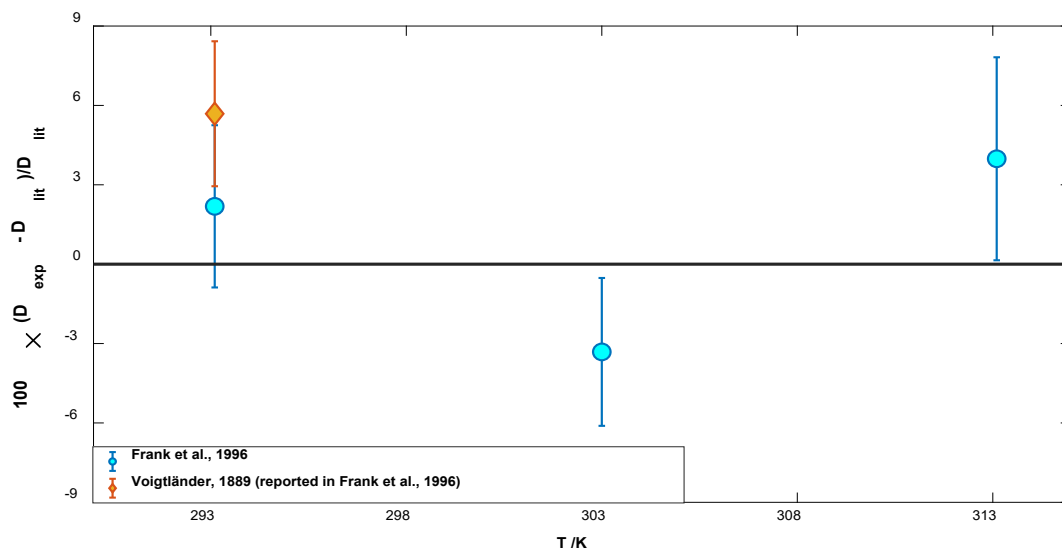
18   *Figure 9. Deviation plot of the mass diffusivity of ammonia in water at different*
19   *temperatures*

22

As shown in Figure 9, the relative deviations between our values and those obtained by Frank et al. [28] do not exceed 4%. Furthermore, the deviations fall within the uncertainty range of the measurements, which highlights the excellent concordance between both studies. Also shown in Figure 9 is the deviation from the study by Voigtländer (reported in Frank et al. [28]) at 293 K. As can be seen, in this case, the deviation is greater, close to 6%, which is still a reasonable value despite the age of the reported data.

As mentioned, the ODI method in combination with an appropriate mass diffusion model is a powerful tool that can simultaneously determine the mass diffusivity (D_{12}) and mass transfer coefficient (k) from a single experimental test. These parameters can be used to determine the mass-transfer Biot number (k_D) defined as [22,23]:

$$k_D = \frac{k * z_0}{D_{12}} \tag{16}$$

Physically, $1/k_D$ represents the ratio of the interfacial resistance ($1/k$) for the mass transfer to the bulk resistance (z_0/D_{12}) for molecular diffusion. For the three experimental temperatures studied, $1/k_D$ ranges from 2.16 x 10^{-3} to 2.56 x 10^{-3}, which indicates that the interfacial resistance is smaller than the resistance for molecular diffusion.

6. Conclusions and perspectives

In this study, we reported the development and implementation of Optical Digital Interferometry (ODI) for visualizing and modelling the mass diffusion in the absorption process of ammonia in water. For this purpose, a new experimental setup was implemented that was based on the Pressure Drop Method with interferometric probing using a Mach-Zehnder interferometer. Absorption experiments were performed at infinite dilution of ammonia and 293 K, 303 K, and 313 K. The experimental procedure, the mathematical formalism, and the main image processing steps of the ODI method for visualizing the mass diffusion layer and determining the experimental profiles of the ammonia concentration in the ammonia/water mixture are described in detail.

A model based on the 1D Fick's Second Law was used to describe the experimental profiles of ammonia concentration. The mass diffusion model used

considered a non-equilibrium boundary condition at the vapour-liquid interface. It was found that the model can successfully reproduce the experimental profiles of the ammonia concentration in the mixture studied. The method developed made it possible to simultaneously determine the mass diffusivity and mass transfer coefficient from a single experimental test. We found that the mass diffusivity of ammonia in water ranged from 1.54×10^{-9} m^2 s^{-1} at 293.1 K to 2.50×10^{-9} m^2 s^{-1} at 313.1 K. The relative deviations between the experimental mass diffusivity and literature values did not exceed 6.0%. The mass transfer coefficient ranged from 2.12×10^{-5} m s^{-1} at 293.1 K to 4.19×10^{-5} m s^{-1} at 313.1 K.

The results obtained in this study show the potential of the method for investigating mass transfer processes in transparent binary mixtures of natural refrigerants with absorbent substances. Optical Digital Interferometry provides new and valuable space-time experimental data on the absorption process, which are useful for developing and validating heat and mass transfer models for designing absorbers and other components in absorption refrigeration systems.

Acknowledgements

Appendix A: Influence of thermal and other *"unwanted"* effects on the refractive index variations

The absorption process of ammonia vapour in water is known to be exothermic. Thus, the evaluation of the absorption thermal effects is fundamental for the method developed in this study because temperature variations can also induce variations in the refractive index. Furthermore, in vapour-liquid absorption experiments, a critical issue in diffusion measurements is to avoid the appearance of convection currents in the liquid phase. In this appendix, the influence of thermal and other *"unwanted"* effects on the refractive index variations are considered and analysed.

1 At low-to-moderate pressures and a given wavelength λ, the total change in the

2 refractive index of liquid mixtures includes temperature, $\Delta T(z,t)$, and

3 concentration, $\Delta C(z,t)$, contributions [10]:

4 $$\Delta n_{\text{Total}}(z,t) = \left(\frac{\partial n}{\partial T}\right)_{C_0,\lambda} \Delta T(z,t) + \left(\frac{\partial n}{\partial C}\right)_{T_0,\lambda} \Delta C(z,t) \qquad \text{(A.1)}$$

5 where T_0 and C_0 are the temperature concentration at reference time, t_{ref}, and

6 the derivative terms (called optical contrast factors) represent the variation of

7 the refractive index with these properties, respectively.

8 **A.1 Influence of thermal effects**

9 Illustratively, the time evolution of the temperature of mixture studied during the

10 absorption process at 313.1 K is shown in Figure A.1. As can be seen, the

11 temperature rises immediately after the ammonia vapour and water in the

12 absorption cell come into contact, reaches a maximum value in a short time,

13 then gradually decreases, and finally remains constant. Note that the final

14 temperature was slightly different (around +0.3 K) to the initial temperature of

15 the experiment. This temperature difference was caused by the limited capacity

16 of the thermal control system and considered in the uncertainty analysis.
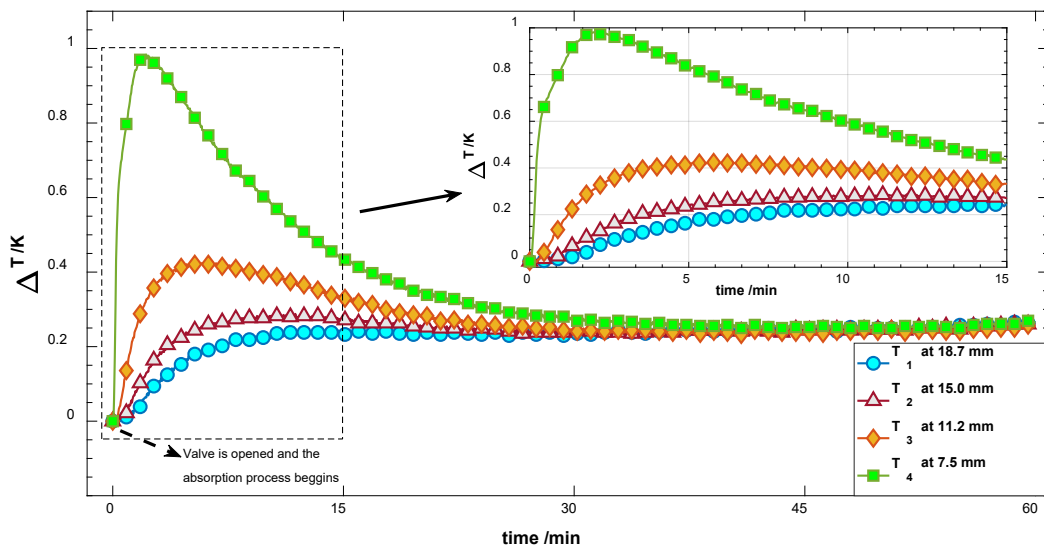
17

18 *Figure A.1. Time evolution of the temperature rise (ΔT) at different distances from the*
19 *vapour-liquid interface inside the ammonia/water mixture during the absorption process*
20 *at 313.1 K. T_1, T_2, T_3, and T_4, represent the temperature probes located in the*
21 *absorption cell within the ammonia/water mixture.*

22 Unlike the mass diffusion layer, the thermal layer should not have a *"preferred"*

23 direction due to the design of the external thermal control system, which

1 extracts heat from the ammonia/water mixture through all the vertical walls of
2 the absorption cell. Moreover, since the thermal diffusivity is much larger
3 (around 60 times at 313.1 K) than the mass diffusivity for the ammonia/water
4 mixtures studied, the thermal layer should be much larger than the mass
5 diffusion layer. In this sense, Mahmoud et al. [5] found that the thermal layer
6 was between 6.4 and 8.5 times larger than the mass diffusion layer. Thus,
7 depending on the absorption time analysed, the increase in temperature can be
8 considered homogeneous in the observation window. Wylock et al. [7] also
9 reached this conclusion based on numerical simulations for the absorption
10 process of CO_2 in an aqueous solution of $NaHCO_3$-Na_2CO_3 in a Hele-Shaw cell
11 visualized by digital holographic interferometry.

12 A homogeneous increase in the temperature of the ammonia/water mixture will
13 affect the total value of the change in the refractive index of the mixture but will
14 not disturb the shape of the profiles. In other words, it will affect the value of Δn_0
15 (factor of proportionality in Eq. (13)) but not that of D_{12} (mass diffusivity) and k
16 (mass transfer coefficient). Note that the term in Eq. (13) that depends on D_{12}
17 and k always varies between 0 and 1, while the value of Δn_0 depends on the
18 experimental conditions studied (temperature, concentration, etc.).

19 To determine the absorption time in which the temperature increase in the
20 observation window can be considered homogeneous, we tentatively used
21 Figure A.1. The observation window was around 8.2 mm from the vapour-liquid
22 interface. Thus, only the temperature probe T_4, located 7.5 mm from the
23 interface, is within the observation window. Nonetheless, the readings of the
24 temperature probes T_1, T_2, and T_3 were useful to get an idea of the thermal
25 homogeneity of the ammonia/water mixture within the absorption cell.

26 As shown in Figure A.1, the greatest temperature variations occur in the first 15
27 minutes of the absorption process. The maximum rise in temperature detected
28 by T_4 was approximately 1 K for an absorption time between 2 and 3 minutes.
29 The extent of temperature rise perceived by probes T_1, T_2, and T_3 located at
30 greater distances from the interface was generally much less and occurred at
31 longer absorption times. For an absorption time of 15 minutes, the difference
32 between T_4 and T_1 (the probes closest and furthest from the interface,
33 respectively) was less than the temperature uncertainty (±0.3 K). Therefore,

1 after 15 minutes, the temperature of the ammonia/water mixture inside the
2 absorption cell can be considered homogeneous.

3 For absorption times less than 15 minutes, the existing temperature gradient in
4 the ammonia/water mixture could have affected the shape of the refractive
5 index profiles (and consequently, the values of D_{12} and k). Intuitively, the rise in
6 temperature of the ammonia/water mixture can be expected to be greatest near
7 the interface. Nonetheless, after a few seconds, Mustafa [6] observed that the
8 temperature rise at the interface decreased rapidly and was reduced by 60%
9 and 80% for absorption times of 5 and 10 minutes, respectively. Moreover,
10 unlike our experimental setup, the setup used by Mustafa [6] did not include an
11 external thermal control circuit. Therefore, the reduction in temperature rise at
12 the interface for our absorption experiments can be expected to be greater for
13 the same absorption times.

14 To get a rough idea of the extent of the thermal effects on the refractive index
15 change profiles, Figure A.2 shows the measured and extrapolated temperature
16 profiles in the ammonia/water mixture. The extrapolated profiles at a distance
17 from the interface between 0 mm < z < 7.5 mm were obtained from the trend of
18 the measured temperature at a distance between 7.5 mm < z < 18.7 mm.
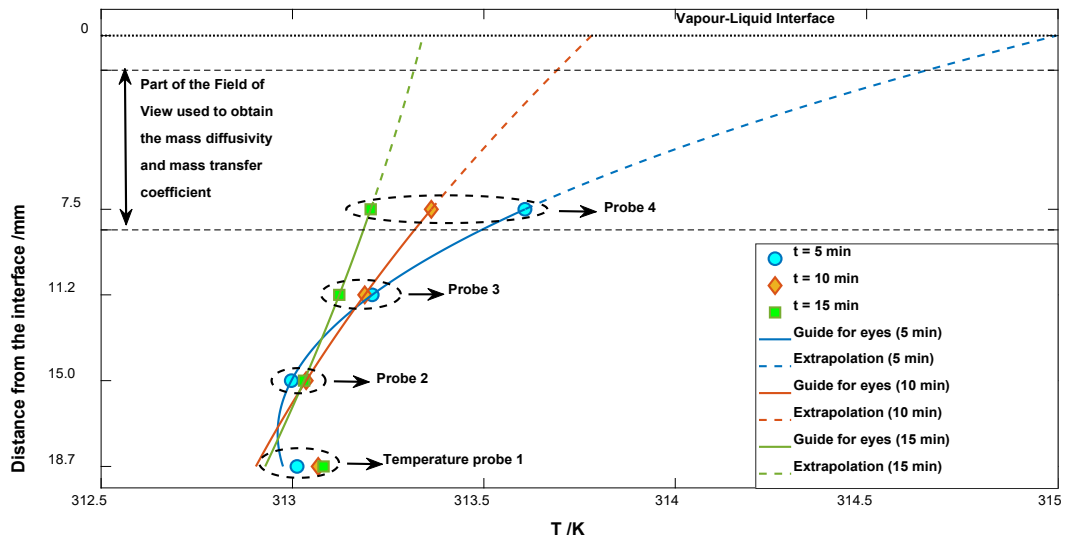
19
20 Figure A.2. Measured and extrapolated temperature profiles at three different
21 absorption times (5, 10, and 15 minutes) during the absorption process of ammonia
22 vapour in water at an initial temperature of 313.1 K.

23 Possible evidence of the adequacy of this extrapolation are:

- For an absorption time of 5 minutes and an initial temperature of 295 K, the increase in temperature at the interface observed by Mustafa [6] was close to 4 K. However, the heat of absorption of ammonia in water decreases with increasing temperature and therefore the temperature increase should be less for a higher initial temperature. Furthermore, in our experiments it is also necessary to consider the cooling action of the thermal control system. Accordingly, for an absorption time of 5 minutes and an initial temperature of 313.1 K, the extrapolation results, showing an increase in interface temperature of 2 K (Figure A.2), appear to be physically consistent with what can be expected from the results provided by Mustafa [6].
- For very short absorption times, Mahmoud et al. [5] observed an exponential behaviour of the temperature profile in the ammonia/water mixture. As the absorption process progressed, the temperature profile adopted a linear behaviour. This thermal behaviour is consistent with that shown in Figure A.2.

On the assumption that the refractive index variation due to temperature variation for the wavelength used (λ = 632.8 nm) and the studied mixtures (infinitely dilute ammonia/water solutions) can be estimated using the relationship found in Wylock et al. [7]:

$$\left(\frac{\partial n}{\partial T}\right)_{C_0,\lambda} = -0.985 \times 10^{-4} \, K$$ (A.2)

the extent of the thermal effects on the refractive index change (Δn_T) was calculated as:

$$\Delta n_T(z,t) = \left(\frac{\partial n}{\partial T}\right)_{C_0,\lambda} \Delta T(z,t)$$ (A.3)

The values of Δn_T in the observation window were 1.14 x10^{-4}, 0.36 x10^{-4}, and 0.13 x10^{-4} for absorption times of 5, 10, and 15 minutes, respectively. These values represented the 39.1%, 7.9%, and 2.5% of the total change (Δn_{Total}) in the refractive index observed in our experiments. Thus, for an absorption time of 5 minutes, the refractive index profiles can be expected to *"deform"* near the vapour-liquid interface (please, see Figure 6) since the share ($\Delta n_T / \Delta n_{Total}$) of the thermal effects was higher there. For absorption times between 5 and 10

28

minutes, this share was reduced five times. For absorption times greater than 10 minutes, the change in refractive index due to temperature variation was one order of magnitude lower than the total change in the refractive index. Thus, we can conclude that the thermal effects on the refractive index fields varied over time, although they are significant at the beginning of the absorption process, they can be neglected after a certain absorption time.

Based on the above, we have selected suitable intervals of absorption time to extract quantitative information from the raw experimental results. For example, the refractive index change profiles observed for absorption times less than 5 minutes were always excluded in the regression procedure to determine the mass diffusivity (D_{12}) and mass transfer coefficient (k). This is because the thermal effects on the refractive index were greater in this interval of absorption times. For absorption times between 5 and 10 minutes, the contribution of thermal effects to the total change in the refractive index was still significant. Despite this, the contribution of thermal effects was much smaller than those related to changes in concentration. In addition, in the determination of D_{12} and k, many more profiles corresponding to absorption times greater than 10 minutes were used. Therefore, in the present study, this marginal contribution of thermal effects to the total change in the refractive index of the ammonia/water mixture was considered in the uncertainty of the reported results.

A.2 Influence of other effects

In addition to thermal effects, other *"unwanted"* effects may cause variations in the refractive index of the ammonia/water mixture. For example, the evaporation of water can induce surface tension gradients along the interface that ultimately lead to a surface driven flow, known as Marangoni convection [29]. Marangoni convection in the ammonia/water absorption process with/without heat transfer additives has been studied using holographic interferometry by Kang and Kashiwagi [4]. The authors observed Marangoni convection near the vapour-liquid interface only in the cases with heat transfer additive. In perfect compliance with the above, here, no Marangoni convection was observed in any of the experiments performed.

The absorption process of ammonia in water always led to a decrease in the density of the liquid phase. Therefore, density-driven natural convection did not occur in our experiments either. It is important to note that this is not the general case, and the possible occurrence of convective currents must be investigated before using the method developed to study the absorption process if the mass diffusivity for a particular mixture is to be determined.

References

[1]   J.D. Killion, S. Garimella, A critical review of models of coupled heat and mass transfer in falling-film absorption, Int. J. Refrig. 24 (2001) 755–797. doi:10.1016/S0140-7007(00)00086-4.

[2]   M. Kojima, T. Kashiwagi, Mass Diffusivity Measurements for Ammonia-Vapour Absorption Processes, in: 19th Int. Congr. Refrig., 1995: pp. 353–360.

[3]   Y.T. Kang, A. Akisawa, T. Kashiwagi, Visualization and model development of Marangoni convection in NH3–H2O system, Int. J. Refrig. 22 (1999) 640–649. doi:10.1016/S0140-7007(99)00019-5.

[4]   Y.T. Kang, T. Kashiwagi, Heat transfer enhancement by Marangoni convection in the NH3-H2O absorption process, Int. J. Refrig. 25 (2002) 780–788. doi:10.1016/S0140-7007(01)00074-3.

[5]   I. Mahmoud, K. Ishida, M. Monde, Analysis of ammonia vapor absorption into ammonia water mixtures: Mass diffusion flux, Heat Mass Transf. Waerme- Und Stoffuebertragung. 41 (2005) 875–889. doi:10.1007/s00231-004-0583-8.

[6]   H. Mustafa, Experimental and Analytical Investigation of Ammonia Vapor Absorption Into a Ammonia-Water Solution, Doctoral Thesis, Saga University, 2007. https://core.ac.uk/download/pdf/59164102.pdf.

[7]   C. Wylock, S. Dehaeck, T. Cartage, P. Colinet, B. Haut, Experimental study of gas-liquid mass transfer coupled with chemical reactions by digital holographic interferometry, Chem. Eng. Sci. 66 (2011) 3400–3412. doi:10.1016/j.ces.2011.01.024.

[8]   Y. Kanda, E. Shoji, L. Chen, J. Okajima, A. Komiya, S. Maruyama, Measurement of transient heat transfer in vicinity of gas–liquid interface using high-speed phase-shifting interferometer, Int. Commun. Heat Mass Transf. 89 (2017) 57–63. doi:10.1016/j.icheatmasstransfer.2017.09.020.

[9]   MATLAB and Image Processing Toolbox Release 2019b, The MathWorks, Inc.,

1   Natick, Massachusetts, United States., (n.d.).

[10]   A. Mialdun, V. Shevtsova, Measurement of the Soret and diffusion coefficients for benchmark binary mixtures by means of digital interferometry, J. Chem. Phys. 134 (2011) 1–12. doi:10.1063/1.3546036.

[11]   A. Mialdun, V. Yasnou, V. Shevtsova, Measurement of isothermal diffusion coefficients in ternary mixtures using counter flow diffusion cell, Comptes Rendus - Mec. 341 (2013) 462–468. doi:10.1016/j.crme.2013.02.001.

[12]   A. Ahadi, M.Z. Saghir, The microgravity DSC-DCMIX1 mission onboard ISS: Experiment description and results on the measurement of the Soret coefficients for isobutylbenzene, dodecane, tetralin ternary hydrocarbons mixtures, Exp. Therm. Fluid Sci. 74 (2016) 296–307. doi:10.1016/j.expthermflusci.2015.12.020.

[13]   R. Rives, A. Mialdun, V. Yasnou, V. Shevtsova, A. Coronas, Experimental determination and predictive modelling of the mutual diffusion coefficients of water and ionic liquid 1-(2-hydroxyethyl)-3-methylimidazolium tetrafluoroborate, J. Mol. Liq. 296 (2019) 111931. doi:10.1016/j.molliq.2019.111931.

[14]   T. Janzen, S. Zhang, A. Mialdun, G. Guevara-Carrion, J. Vrabec, M. He, V. Shevtsova, Mutual diffusion governed by kinetics and thermodynamics in the partially miscible mixture methanol + cyclohexane, Phys. Chem. Chem. Phys. 19 (2017) 31856–31873. doi:10.1039/c7cp06515a.

[15]   R. Rives, Theoretical and Experimental Study of the Absorption Process of Ammonia in Ionic Liquids for Absorption Refrigeration Systems, Doctoral Thesis, Universitat Rovira i Virgili, 2021. http://hdl.handle.net/10803/670713.

[16]   M. Takeda, H. Ina, S. Kobayashi, Fourier-transform method of fringe-pattern analysis for computer-based topography and interferometry, J. Opt. Soc. Am. 72 (1982) 156. doi:10.1364/JOSA.72.000156.

[17]   T. Kreis, Digital holographic interference-phase measurement using the Fourier-transform method, J. Opt. Soc. Am. A. 3 (1986) 847–855. doi:10.1364/JOSAA.3.000847.

[18]   M.A. Rahman, M.Z. Saghir, Ground based measurement and theoretical calculation of Soret coefficient of binary hydrocarbon mixtures, Exp. Therm. Fluid Sci. 49 (2013) 31–39. doi:10.1016/j.expthermflusci.2013.03.008.

[19]   M.B. Shiflett, A. Yokozeki, Solubilities and diffusivities of carbon dioxide in ionic liquids: [bmim][PF6] and [bmim][BF4], Ind. Eng. Chem. Res. 44 (2005) 4453–4464. doi:10.1021/ie058003d.

[20] H.M. Ariyadi, A. Cera-Manjarres, A. Coronas, Absorption Behaviour and Diffusivity of Ammonia in Ionic Liquids, in: 5th IIR Int. Conf. Thermophys. Prop. Transf. Process. Refrig., International Institute of Refrigeration, Seoul, South Korea, 2017: pp. 1–8. doi:10.18462/iir.tptpr.2017.0129.

[21] Y.P. Zhang, C.L. Hyndman, B.B. Maini, Measurement of gas diffusivity in heavy oils, J. Pet. Sci. Eng. 25 (2000) 37–47. doi:10.1016/S0920-4105(99)00031-5.

[22] S.R. Etminan, B.B. Maini, Z. Chen, Determination of mass transfer parameters in solvent-based oil recovery techniques using a non-equilibrium boundary condition at the interface, Fuel. 120 (2014) 218–232. doi:10.1016/j.fuel.2013.11.027.

[23] A.K. Tharanivasan, C. Yang, Y. Gu, Comparison of three different interface mass transfer models used in the experimental measurement of solvent diffusivity in heavy oil, J. Pet. Sci. Eng. 44 (2004) 269–282. doi:10.1016/j.petrol.2004.03.003.

[24] J. Crank, The Mathematics of Diffusion, 2nd ed., Oxford University Press, Oxford, England, 1975.

[25] S. Zhang, M. He, Y. Zhang, S. Peng, X. He, Study of the measurement for the diffusion coefficient by digital holographic interferometry, Appl. Opt. 54 (2015) 9127–9135. doi:10.1364/ao.54.009127.

[26] MATLAB and Statistics and Machine Learning Toolbox, Release 2018a, The MathWorks, Inc., Natick, Massachusetts, United Sates., (n.d.).

[27] A. Mialdun, V. Sechenyh, J.C. Legros, J.M. Ortiz De Zárate, V. Shevtsova, Investigation of Fickian diffusion in the ternary mixture of 1,2,3,4-tetrahydronaphthalene, isobutylbenzene, and dodecane, J. Chem. Phys. 139 (2013) 104903. doi:10.1063/1.4820357.

[28] M.J.W. Frank, J.A.M. Kuipers, W.P.M. van Swaaij, Diffusion Coefficients and Viscosities of CO_2 + H_2O, CO_2 + CH_3OH, NH_3 + H_2O, and NH_3 + CH_3OH Liquid Mixtures, J. Chem. Eng. Data. 41 (1996) 297–302. doi:10.1021/je950157k.

[29] X. Song, D.S. Nobes, Experimental investigation of evaporation-induced convection in water using laser based measurement techniques, Exp. Therm. Fluid Sci. 35 (2011) 910–919. doi:10.1016/j.expthermflusci.2011.01.010.